HYDROLYTIC AND ENZYMATIC DEGRADATION OF BIOBASED POLY(4-HYDROXYBUTYRATE) FILMS. SELECTIVE ETCHING OF SPHERULITES.

Ina Keridou[1], Lourdes Franco[1,2], Luis J. del Valle,[1,2] Juan C. Martínez[3], Lutz Funk[4], Pau Turon[4], Jordi Puiggalí[1,2,5*]

[1]Departament d'Enginyeria Química, Universitat Politècnica de Catalunya, Escola d'Enginyeria de Barcelona Est-EEBE, c/Eduard Maristany 10-14, Barcelona 08019, SPAIN

[2]Center for Research in Nano-Engineering, Universitat Politècnica de Catalunya, Campus Sud, Edifici C', c/Pasqual i Vila s/n, Barcelona E-08028, SPAIN

[3]ALBA Synchrotron Light Facility, Carrer de la Llum, 2-26, 08290, Cerdanyola del Vallès, Barcelona, SPAIN

[4]B. Braun Surgical, S.A. Carretera de Terrasa 121, 08191 Rubí (Barcelona), SPAIN

[5]Institute for Bioengineering of Catalonia (IBEC), The Barcelona Institute of Science and Technology, c/Baldiri Reixac 10-12, 08028 Barcelona, SPAIN

Correspondence to: **J. Puiggalí (E-mail: Jordi.Puiggali@upc.edu)**

ABSTRACT

Hydrolytic degradation of poly(4-hydroxybutyrate) (P4HB) films has been studied considering media of different pH values (i.e., 3, 7 and 10) and temperatures (i.e., 37 and 55 ºC). Enzymatic degradation has also been evaluated at physiological conditions using two different lipases: *Pseudomonas cepacia* and *Rhizopus oryzae*.

Different bulk and surface erosion mechanisms with random chain scissions and successive removal of monomer units have been supported through weight loss measurements, molecular weight determinations by GPC and NMR spectroscopy and changes on thermal properties by DSC. Thermal annealing during exposure to different media and even degradation influenced on the melting temperature and crystallinity of samples, as well as on the lamellar geometrical parameters as evaluated by SAXS. Enzymatic degradation was ideal to selectively eliminate the amorphous regions and highlight the spherulitic morphology. Presence of ringed textures were therefore evident in bright field optical micrographs in addition to SEM images, namely observations under polarized light was not necessary to distinguish the presence of banded spherulites. *Rhizopus oryzae* was revealed to be the most suitable enzyme to crop out the P4HB spherulites that form part of the initial smooth surfaces of solvent casting films. After determining the appropriate activity and exposure time, the presence of rings constituted by cooperative C-shaped edge-on lamellae and flat-on lamellae was highlighted.

Keywords: Poly(4-hydroxybutyrate), biodegradable polymers, hydrolytic degradation, enzymatic degradation, films, thermal properties, microstructure.

INTRODUCTION

Poly(4-hydroxybutyrate) (P4HB) is a biodegradable polyester widely employed in biomedical applications due to its biocompatibility and unique properties. Specifically, P4HB is considered for developing long-term sutures, abdominal wall closure materials, reconstructive surgery materials, scaffolds, heart valves and vascular grafts among others uses [1–8].

P4HB, like other poly(hydroxyalkanoates) can be produced in high yield from microorganisms (e.g. *Escherichia coli*) in response to nutrient defective conditions [9]. P4HB mainly degrades by surface erosion giving rise to 4-hydroxybutyrate as the main product. This is a common metabolite of the human body and therefore minimum adverse reactions in soft tissues (e.g., abdominal wall and muscles) are derived after implantation. Microbial P4HB has a very high molecular weight ($M_n \sim 10^6$ g/mol) and a remarkable elastomeric character at room and body temperatures. In fact, P4HB can be stretched 10 times its original length before breaking. Other advantages of P4HB correspond to its solubility in organic polar solvents and low melting temperature that facilitate its processing, if it is not compromised by the high molecular weight [10].

Despite the above indicated properties of P4HB, scarce works have been performed on the study of physical properties, crystalline structure, morphology and crystallization processes. This feature contrasts with the exhaustive information concerning to related polyesters (e.g., polyglycolide and poly(ε-caprolactone), which are the most similar ω-hydroxy acid derivatives, constituted also by an even number of carbon atoms in the main chain) or even to other biodegradable polyesters, such as polylactide and poly(3-hydroxybutyrate) (P3HB), which differ on the presence of methyl side groups. The peculiar characteristics of P4HB have enhanced the interest on their copolymers. Thus,

poly (3-hydroxybutyrate-*co*-4-hydroxybutyrate) (P(3HB-co-4HB)) is a widely employed bacterial copolyester where the presence 4-hydroxybutyrate units is fundamental to reduce the stiffness of the P3HB homopolymer [11,12]. Chemical synthesis has also been employed to develop copolyesters based on 4-hydroxybutyrate units [13].

X-ray fiber diffraction data and single crystal electron diffraction patterns pointed out that P4HB crystallizes according to an orthorhombic unit cell with space group $P2_12_12_1$ and parameters: a = 0.775 nm, b = 0.479 nm and c (fibre axis) = 1.194 nm [14,15]. Diffraction data and energy calculations [15] indicated that P4HB molecules crystallized according to a slight distortion of an all-trans conformation. Molecular deformation under uniaxial stretching has been simulated, being suggested that crystalline regions played a fundamental role in the stretching deformation [16].

Concerning to the crystalline morphologies, it should be pointed out that lozenge-shaped multi-terrace crystals can be obtained from crystallization in dilute ethanol solutions at 80 ºC. Growth planes corresponded to {110} planes and the ratio between the two diagonal axes is close to 3:5 [15].

Enzymatic degradation of such single crystals was studied by turbidity assays in lipase medium from *Pseudomonas* sp. and an extracellular PHB depolymerase from *Pseudomonas stutzeri* YM1006 [15]. Morphological observations indicated that enzymatic attack took place from the crystal edges since both molecular weight and lamellar thickness remained unchanged. This feature, suggested that chain-folding regions on the lamellar surface were unaltered. Nevertheless, evidences that enzymatic degradation had also occurred at the folded chain region of single crystal surfaces have been found for P(3HB-co-4HB) copolymers [17].

P4HB crystallized from the melt and also from chloroform solutions as negative ringed spherulites [18,19]. Rings were distinguished by highly zigzag irregularities and had

different widths depending on birefringence (i.e., the dark and non-birefringent rings were the narrowest). Analysis of thin spherulites obtained by solvent casting by infrared microspectroscopy was not conclusive about molecular orientation differences in dark and bright rings [18]. Therefore, reported experimental data were not useful to discern between the two typical explanations formulated, to elucidate the ringed morphology of spherulites. Namely, a continuous twisting of constitutive lamellae [20] or alternatively a rhythmic growth derived from the presence of depletion zones in the growth front [21].

Partial degradation of P4HB films in a lipase from *Pseudomonas* sp. medium (24 h at 37 °C) revealed the apparition of spherulites without a defined texture, while experiments performed with stretched films showed the apparition of shish-kebab morphologies, both features as consequence of a faster erosion of amorphous regions and the cropping out of crystal regions [15].

The main goal of the present work is to insist on the study of degradation of melt pressed films considering different media and conditions. Specifically, the evaluation of the impact of degradation on crystalline and amorphous regions will be considered. The expected preferential attack on the amorphous phase appears as a relevant feature that can be employed to highlight spherulitic characteristics when surface erosion is favoured.

EXPERIMENTAL SECTION

Materials

Commercially available samples of P4HB (Monomax ™, USP 1) were kindly supplied by B. BRAUN Surgical S.A. Weight and number average molecular weights of these samples were 215,000 and 68,000 g/mol, respectively, as determined by GPC. *Pseudomona cepacia* and *Rhizopus oryzae* enzymes with specific activity of 40.0 and 55.7 U/mg solid,

respectively, were obtained from Sigma-Aldrich (Spain). All reagents, chloride acid (HCl) and chloroform ($CHCl_3$) were provided from Fisher Chemical (U.S).

Hydrolytic degradation

In vitro hydrolytic degradation studies were performed at 37 ºC and 55 ºC to simulate human body conditions and compost media. Studies were performed with films with dimensions of 1 cm × 1 cm × 150 μm, which. These films were obtained by melt pressing (5 bar) at a temperature of 60 ºC, and a subsequent spontaneous cooling to room temperature where they remained for 5 min. *In vitro* hydrolytic degradation studies were performed at 37 ºC and 55 ºC to simulate human body conditions and compost media. Studies were performed with films with dimensions of 1 cm × 1 cm × 150 μm, which were pressed (5 bar) and melted at temperature of 60 ºC. Assays were carried out at the two indicated temperatures in different pH values of 3, 7 and 10 using the Universal buffer (citrate-phosphate-borate/HCl) solution [22]. This buffer was prepared by mixing 20 mL of the stock solution with *x* mL of 0.1 M HCl and distilled water up to 100 mL. The stock solution (1 L) contained 100 mL of citric acid, 100 mL of phosphoric acid, 3.54 g of boric acid and 343 mL of 1M NaOH. Therefore, the buffers of pH 3, pH 7 and pH 10 values were obtained by mixing 20 mL of the stock solution and 56.9, 32.9 and 18.1 mL of 0.1 M HCl, respectively. Samples were kept under orbital shaking in bottles filled with 50 mL of the degradation medium and sodium azide (0.03 wt-%) to prevent microbial growth for selected exposure times. The samples were then thoroughly rinsed with distilled water, dried to constant weight under vacuum and stored over P_4O_{10} before analysis. Weight retention was evaluated during degradation as well as the changes on molecular weight. Degradation studies were performed in triplicated and the given data corresponded to the average values.

Enzymatic degradation

Enzymatic degradation studies were performed at 37 ºC with melt pressed films having the above indicated dimensions. Indeed, according to *Boesel et al.* the bacterial synthesis of P4HB

usually leads up to very high molecular weight (M_n ~ 10^6 g/mol), however the Monomax suture (commercialized product) which was used to prepare the films is derived from poly-4-hydroxybutyrate homopolymer, which is produced by Tepha, Inc. (Lexington, MA, USA). Tepha, Inc. produces P4HB using a proprietary transgenic fermentation process utilizing a genetically engineered *Escherichia coli* K12 microorganism that incorporates new biosynthetic pathways to produce the homopolymer. The advantage of this fermentation approach is the control of the molecular weight, because the varied activities of specific pathway enzymes within the cells are in dependence with the molecular weight. Studies were carried out in media containing lipases from *Pseudomonas cepacia* (0.1 mg/mL) and *Rhizopus oryzae* (0.072 mg/mL). All samples were exposed to 1 mL of phosphate buffered saline (PBS) (pH 7.4) containing the determined enzyme alongside with sodium azide (0.03% w/v). These solutions were renewed every 48 h to prevent enzymatic activity loss. Samples were kept at 37 °C in an orbital shaker at 80 rpm. Samples were taken from the media at determined times, washed three times with Milli-Q water and dried in an oven at 37 °C for 24 h to determine the dry weight. All the experiments were conducted in triplicate. The degraded samples were carbon coated and observed in SEM with an accelerating voltage of 10 kV.

Measurements

Weight loss (W_l) of the specimens was determined through equation 1 where W_d is the sample weight after degradation and W_0 is the initial simple weight, i.e., before exposure to the degradation medium:

$$W_l = 100 \times (W_0 - W_d) / W_o \qquad (1)$$

Molecular weight was estimated by size exclusion chromatography (GPC) using a liquid chromatograph (Shimadzu, model LC-8A) equipped with an Empower computer program (Waters). A PL HFIP gel column (Polymer Lab) and a refractive index detector (Shimadzu RID-10A) were employed. The polymer was dissolved and eluted in 1,1,1,3,3,3-hexafluoroisopropanol (HFIP) containing CF_3COONa (0.05 M) at a flow rate of 0.5 mL/min

(injected volume 100 μL, sample concentration 2.0 mg/mL). Number and weight average molecular weights were calculated using polymethyl methacrylate standards.

^{1}H-NMR spectra were acquired with a Bruker NMR Ascend 400 spectrometer operating at 400 MHz. Chemical shifts were calibrated using tetramethylsilane as an internal standard. Deuterated chloroform was used as the solvent.

Calorimetric data were obtained by differential scanning calorimetry with a TA Instruments Q100 series equipped with a refrigerated cooling system (RCS) operating at temperatures from -50 ºC to 150 ºC. Calibration was performed with indium. Experiments based on heating runs at 10ºC/min were conducted under a flow of dry nitrogen with a sample weight of approximately 5 mg.

WAXD and SAXS data were obtained at the NCD beamline (BL11) of the ALBA synchrotron facility (Cerdanyola del Vallès, Barcelona, Spain), by using a wavelength of 0.100 nm. A WAXD LX255-HS detector from Rayonix and an ImXPAD S1400 photon counting detector were employed. Polymer samples were confined between Kapton films. WAXD and SAXS diffraction patterns were calibrated with Cr_2O_3 and silver behenate (AgBh), respectively. The correlation function and the corresponding parameters were calculated with the CORFUNC software for Fibre Diffraction/Non-Crystalline Diffraction provided by the Collaborative Computational Project 13. Deconvolution of WAXD peaks was performed using the PeakFit 4.0 software.

Spherulite cropping out by enzymatic degradation

Spherulites were grown from homogeneous thin films prepared by evaporation of dilute solutions of the polymer in $CHCl_3$ (0.01 g/mL). The films were dried at vacuum until a constant weight was achieved. The prepared thin films were exposed to both *Pseudomonas cepacia* (0.1 mg/mL) and *Rhizopus oryzae* (0.072 mg/mL) enzymatic

media during different exposure times. Samples were subsequently washed three times with Milli-Q water and dried in an oven at 37 °C for 24 h to determine the dry weight.

Bright field and polarized optical micrographs were taken with a Zeiss Axioskop 40 Pol light polarizing microscope. A first-order red tint plate was employed to determine the sign of spherulitic birefringence under crossed polarizers.

Scanning electron micrographs were taken using a Phenom XL Desktop SEM equipment. Degraded films were mounted on a double-sided adhesive carbon disc and were sputter-coated with a thin layer of carbon to prevent sample charging problems using a K950X Turbo Evaporator. All samples were observed at an accelerating voltage of 10 kV.

Statistical Analysis

Values were averaged and graphically represented together with their respective standard deviations. Statistical analysis was performed by one-way ANOVA test to compare the means of all groups, and then Tukey's test was applied to determine a statistically significant difference between two groups. The test confidence level was set at 95% ($p < 0.05$).

RESULTS AND DISCUSSION

Hydrolytic degradation of P4HB films

Hydrolytic degradation of P4HB is a bulk process that is influenced by the pH of the medium and obviously by temperature. The evolution of weight loss and molecular weight have been evaluated at representative pH values of 3, 7 (close to physiological) and 10 and temperatures of 37 ºC (physiological) and 55 ºC (maximum allowed value before to start the melting process). Figure 1a shows that the degradation at 37 ºC is not significant when only the weight loss is considered. Note that, only a small weight loss that reaches a value lower than 0.2% can be detected during the 3 first days of exposure and that probably corresponds to

additives, like typical colorants and very small fragments that have been incorporated to the commercial sample. The behaviour is different at 55 ºC where a loss of material around 2.1% can be determined for the pH 10 medium suggesting a very small degradation process. Results were again not significant at the other two pH values (i.e., around 0.6% after 3 days of exposure at pH 3 and around 0.7% after 21 days at pH 7). It is evident, as well-reported, that hydrolytic degradation of P4HB is a slow process that leads to few small and soluble fragments. Obviously, these are the only ones that can be detected through simple weight loss measurements and become originated from a depolymerization process, which seems not favoured. Logically, solubilization of these small fragments having carboxylate end groups, can only be significant at basic pH media.

Nevertheless, GPC measurements allowed confirming that degradation is relatively significant at 55 ºC and even at 37 ºC since a reduction of molecular weight is clearly detected (Figure 1b). In this case, the more aggressive medium corresponds to the acidic pH, demonstrating the contradictory conclusions that could be derived if only the weight loss of material is taken into account. Random chain scissions seem to be the preferential degradation mechanism and consequently, small soluble fragments are produced in agreement with weight loss measurements. An important conclusion is that a preferential attack over the amorphous domains in polymer films cannot be easily detected by simple morphological observations, due to both a bulk erosion and scarce production of soluble fragments.

NMR spectra allowed estimating also the number average molecular weight of exposed samples to hydrolytic degradation media. In this case, measurements have the advantage of being independent of the solution molecular chain conformation and the appropriate selection of the GPC calibration standard, although some imprecision is expected for samples with high molecular weight (e.g., M_n higher than 10,000 g/mol). Figure 1c displays

a typical spectrum of a representative sample, where in addition to the proton signals of the three CH_2 groups of the main chain repeat unit at 4.08 ppm (OCH_2, t), 2.35 ppm (CH_2CO, t) and 1.94 ppm (OCH_2CH_2, m), small signals associated to terminal groups can be observed. Thus, M_n could also be estimated taken into account the intensity ratio between signals at 4.08 ppm and 4.29 ppm (CH_2OH, t):

$$M_n \text{ (g/mol)} = 86*I_{4.08}/I_{4.29} + 87+103 \qquad (1)$$

where 86, 87 and 103 are the molecular weights of the repeat unit, the hydroxyl terminal group and the carboxyl terminal group, respectively.

NMR results indicate a molecular weight dependence with medium pH that is in full agreement with that observed from GPC measurements, although values are usually higher. Only data corresponding to the lower molecular weights (i.e., degradation at 37 ºC and 55 ºC during 14 and 27 days) are plotted in Figure 1b and summarized in the supporting information section.

Enzymatic degradation of P4HB films

Degradation in lipase media was clearly more efficient, as can be detected in the SEM micrographs taken after 27 days of exposure. Assays were performed using *Pseudomonas cepacia* and *Rhizopus oryzae* enzymes, where different susceptibility of P4HB films towards the indicated enzymes is clear. It should be pointed out that the surface of films is clearly more eroded using *Rhizopus oryzae*, a feature that evidences the capacity to finely tune the degradation by the selection of the appropriate enzymes. The surface of films used as control was practically not affected due to the scarce hydrolytical degradation at 37 ºC. Micrographs depict also the presence of crystals produced from degradation products that evidenced the problems associated with their low solubility (Figure 2a).

In contrast with results attained using hydrolytic media, Figure 2b demonstrates the highly significant weight loss of exposed samples (e.g., 25% and 40% after 7 days of exposure to

Pseudomonas cepacia and *Rhizopus oryzae* media, respectively). A practically complete degradation (i.e., 95%) was even produced after only 21 days of exposure to the most aggressive medium. These high weight loses were observed despite that the solubility problems remain and that the erosion is a surface process instead of a bulk degradation. Results suggest that a selective erosion of amorphous regions can be achieved through appropriate selection of an enzyme and exposure time.

Figure 2c compares the GPC molecular weights of samples exposed to both enzymatic media and the control (pH 7.4 aqueous medium). In this case, differences between hydrolytic and enzymatic degradation is not so noticeable than those deduced from the weight loss measurements. It is evident that degraded fragments are retained in the bulk-eroded sample and probably a different chain scission mechanism exists (i.e., random chain scission for the hydrolytic process and depolymerization or successive removal of monomer units for the enzymatic one). Molecular weight results were again in agreement with a preferential degradation on the *Rhizopus oryzae* medium.

Thermal properties of hydrolytically and enzymatically P4HB degraded samples

Fusion of the P4HB homopolymer is characterized by a double melting peak, as shown in the left inset of Figure 3a. This complex fusion has been associated to the existence of two lamellar populations with different thicknesses since no polymorphic forms have been described for P4HB [18]. Temperatures of the melting peaks are susceptible to thermal annealing processes since clear differences have been reported [18] between melt crystallized sample and annealed sutures. Specifically, the temperature of the lower (T_{m1}) and the main (T_{m2}) melting peak can be increased from 58 ºC to 72 ºC and from 50 ºC to 62 ºC, respectively.

P4HB films exposed to hydrolytic degradation showed a significant change in thermal properties (i.e., T_{m1}, T_{m2} and melting enthalpy) as summarized in Table 1. Interpretation of

the observed changes is difficult since annealing effects derived from exposure to different temperatures, times and media may play a significant role and mask those effects attributed to the potential degradation of molecular chains. Nevertheless, experimental data allow us to perform the following conclusions:

a) Thermal annealing caused a significant increase on the melting temperatures as shown in the left inset of Figure 3a that compares the DSC traces of the initial sample and films exposed for 27 days to a pH 10 representative media at 37 ºC and 55 ºC. According to Table 1, T_{m1} increased from 49.7 ºC (initial film and 25 ºC) to 53.2-59.0 ºC after exposure to the media at 37 ºC, and T_{m2} increased from 58.2 ºC (initial film at 25 ºC) to 59.5-63.3 ºC and 71.4-75.9 ºC for media at 37 ºC and 55 ºC, respectively. Samples hydrolyzed at 55 ºC showed a broad and low intense T_{m1} peak that was produced as consequence of some residual crystallization during the subsequent drying at room temperature. It is obvious that the initial thinner crystals were melted and recrystallized in the degradation media at 55 ºC. Note also that in these media, films could reach a T_{m2} temperature higher that the annealed commercial sutures. An effect caused by degradation could in addition be considered. Namely, degradation of crystalline regions should proceed through the amorphous lamellar folding surfaces giving rise to a significant decrease on the molecular weight as detected at 55 ºC and an increase of the lamellar core thickness and even on the thickness of the amorphous lamellar surface layer.

Melting enthalpy was also clearly influenced by the lamellar reordering process induced by temperature and probably in a minor degree by degradation as discussed in the following points. Thus, the enthalpy of the initial sample (34.5 J/g) increased to 49.1-59.7 ºC and 54.7-70.6 ºC after exposure to media at 37 ºC and 55 ºC, respectively. Note that the observed changes cannot be attributed to degradation and solubilization of amorphous domains as could be deduced by the minimum weight losses indicated in Figure 1.

b) For a given degradation assay melting peak temperatures and melting enthalpy gradually increased with the exposure time. Figure 3a illustrates the evolution of the melting peak for a sample exposed to a pH 10 medium at 55 ºC. In this case, the melting temperature regularly increased from 71.5 ºC to 75.2 ºC as the degradation time increased from 3 to 27 days. In the same way, the melting enthalpy slightly increased from 54.0 J/g to 65.2 J/g. Results indicate a significant increase on the crystallinity of the sample during exposure, as reflected by the variation of enthalpy. A crystallization process may occur as consequence of both the decrease of molecular weight and a time dependent annealing since as indicated the solubilization of amorphous domains is discarded. A regular increase on the lamellar thickness that justifies the observed change on the melting temperature can also be inferred. Change on thermal properties were logically more significant at the higher temperature and for example, the melting enthalpy of samples exposed to the pH 3 medium at 37 ºC and 55 ºC varied from 54.7 J/g to 70.9 J/g (i.e., 16.2 J/g) and from 50.1 J/g to 59.7 J/g (i.e., 9.6 J/g), respectively.

c) The pH of the medium had a slight influence on thermal properties but as a general trend it was observed that both melting peak temperature and melting enthalpy slightly increased whit the decrease of the pH value (Table 1 and right inset of Figure 3a). Thus, samples exposed for 27 days at 37 ºC showed a T_{m2} increase from 63.6 ºC to 64.1 ºC and a melting enthalpy increase from 58.5 J/g to 59.7 J/g when pH decreased from 10 to 3. Similar changes were observed at 55 ºC and specifically temperature increased from 75.2 ºC to 75.9 ºC and the enthalpy from 65.2 J/g to 70.6 J/g. This trend correlates with the observed higher degradation in acidic media.

Figure 3b shows the evolution of DSC heating runs of samples exposed, for increasing times, to the less aggressive *Pseudomonas cepacia* enzymatic medium. Basically, the behavior became similar to that found for the control (i.e., aqueous medium without enzyme and pH

7.4) and clearly demonstrated that this enzymatic degradation has a very small effect on the crystalline regions. A slight shift of the main melting peak (T_{m2}) and the associated shoulder (T_{m1}) can be detected as the exposure time increased (Table 2), but this evolution appears in full agreement with the data corresponding to the hydrolytic degradation. The inset of Figure 3b compares the DSC heating runs of samples exposed to *Pseudomonas cepacia* and the *Rhizopus oryzae* media for the maximum studied exposure of 21 days. In this situation, small differences can be detected and demonstrated that the higher attack of *Rhizopus oryzae* to the amorphous regions leading to a significant weight loss and an small increase on crystallinity (i.e., higher melting enthalpy) with respect to the samples coming from the *Pseudomonas cepacia* medium. It can also be indicated the shift of the T_{m1} shoulder to higher temperatures, a reature that may suggest that the amorphous folding surfaces of the thinner lamellae were more susceptible to the enzymatic attack.

Influence of hydrolytic and enzymatic degradation on the P4HB lamellar thickness

In order to complement the DSC observations, small angle X-ray scattering (SAXS) patterns were also considered to analyse the change on the lamellar morphologies during exposure to the different media and temperatures.

Analysis was performed through the use of the normalized correlation function:

$$\gamma(r) = \int_0^\infty q^2 I(q) \cos(qr) dq \; / \; \int_0^\infty q^2 I(q) dq \qquad (2)$$

where $I(q)$ is the intensity of the SAXS peak at each value of the scattering vector ($q = [4\pi/\lambda] \sin \theta = 2\pi/d$, with θ and d being the Bragg angle and the Bragg spacing, respectively).

Long period, L_γ, amorphous layer thickness, l_a, and crystalline lamellar thickness, l_c, can be determined by the normalized one-dimensional correlation function [23] and applying

the Vonk's model [24] and Porod's law to perform extrapolations to low and high q values.

Figure 4a illustrates 1D-SAXS profiles and the corresponding correlation functions of samples degraded during 27 days at 37 ºC. Differences are significant with respect to the original film and agrees with the previously indicated thermal annealing effect. Nevertheless, correlation functions were practically identical, despite the change of the pH of the medium. In fact, data summarized in Table 3 indicated L_γ, l_c and l_a values of 8.50-8.60, 6.80-6.91 and 1.62-1.70, which means random changes of the three parameters that are lower than 0.12 nm and that have no physical meaning.

Clearer differences were observed with the previous data when degradation was performed at 55 ºC, since L_γ increased significantly to 9.60-9.80 nm and l_c increased to 7.29-7.62 nm (Figure 4b). Note that this evolution is in agreement with the discussed DSC observations that suggested an increase on the lamellar spacing as degradation and annealing temperature were increased. Lamellar parameters of samples degraded at 55 ºC in different pH values were relatively similar, but evidenced a significant increase of l_a from 1.98 nm to 2.48-2.51 nm when pH was lowered. The advance of degradation seems to affect clearly the lamellar folding surfaces, with the corresponding thickness increase being associated to the breakage of chains in the irregular folds and the production of less compact layers. Note also the increase of l_a when samples degraded at 37 ºC and 55 ºC are compared. The shape of the correlation functions also varied and specifically showed that minima and maxima were sharper as the degradation progressed. This feature is consequence of a greater difference between the electronic densities of amorphous and crystalline layers as could be justified from the loosely packing of broken folds.

The change of the correlation function during enzymatic degradation in different media is also shown in Figure 4c and Table 3. Yet again, more degraded samples showed sharper

maxima and minima, and increased L_γ and l_a values. Note for example that the enzymatic degradation for only 14 days (pH 7.4, 37 ºC) in the *Rhizopus oryzae* medium becomes similar to the hydrolytic degradation for 27 days in a pH 3 medium at 55 ºC. This feature suggests that the observed morphological changes were not only a direct consequence of lamellar reordering processes induced by temperature and that degradation played also a highly significant role.

Despite the observed changes in the l_c and l_a values, it should be pointed out that the crystallinity of the lamellar stacks (i.e., $\chi^{SAXS} = l_c / l_\gamma$) is relatively constant and specifically varies between 0.75 and 0.81 without any specific trend (Table 3). The morphology of lamellae changed during annealing and degradation but the corresponding crystallinity does not change significatively in contrast with the global crystallinity of the sample that is affected by the attack, solubilization or recrystallization of the amorphous domains.

Revealing P4HB spherulitic morphologies by enzymatic degradation of thin films

Thin films of P4HB (thickness lower than 10 μm) were prepared as exposed in the materials and methods section. Films were placed to the same enzymatic media, considering the two previously evaluated lipases in order to visualize the morphology of crystalline spherulites developed on the surface of films. The activity of enzymes was however increased (i.e., from 4 to 40 U/mL for both *Pseudomonas cepacia* and *Rhizopus oryzae*) to get sufficiently eroded surfaces within a reasonable time of exposure (i.e., maximum 3 hours).

Figures 5a and 5b show bright field and polarized optical micrographs of the P4HB film initial surface. Bright field image allows detecting the presence of multiple bumps in the film surface, which can be related to the spherulites as clearly observed in the corresponding micrograph taken under polarizers. The observed spherulites had a

variable size with diameters ranging between 20 and 40 μm and a banded texture with a spacing between rings close to 5 μm. A negative birefringence was always detected (see inset of Figure 5b) as characteristic of aliphatic polyesters and as reported for melt crystallized P4HB.

Origin of banded spherulites is a matter motif of controversial with different explanations being postulated. Thus, development of interlamellar screw dislocations or presence of polymorphic structures have been in some cases indicated.

An interesting explanation was also given considering the effects of a rhythmic growth caused by the periodic presence of depletion zones in the crystal growth front [25]. A diffusion rate of the melted polymer, lower than the rate at which chains are consumed to form the crystalline lamellae, leads to these depletion zones. Films having concentric-ringed textures and an alternate disposition of ridges and valleys (i.e., the depletion zones) have been observed in polymers like isotactic polystyrene [26,27]. Moreover, ringed textures constituted by flat on lamellar crystals were characteristic of some solution crystallized thin films and explained in some cases by the rhythmic model (e.g., poly(bisphenol A hexane ether) [28] and poly(ε-caprolactone) [25].

Nevertheless, the most generalized interpretation considers a continuous twisting of constitutive lamellae along the spherulite radius. Imbalanced stresses at the two lamellar folding surfaces have been postulated as the main reason to induce a regular lamellar twisting [29]. Imbalances can be a consequence of the presence of chiral units (e.g., poly(3-hydroxybutyrate) [30] and isotactic poly(1-butene) [31]), chain tilt respect to the lamellar surface (e.g. polyethylene [32,33]), asymmetric repeat units (e.g., ω-hydroxy acid derivatives like polypivalolactone [34]) and differences on the folding units (e.g., nylon 6,6 [35] and poly(vinylidene fluoride) [36], which lead in this case to a lamellar scrolling). Lamellar twisting can also be deduced from SEM micrographs of melt

crystallized spherulites after chemical etching [37] (e.g., polyethylene [38]) where cooperative C-shaped lamellar edges (or alternatively inverted C-shaped edges depending on the handle sense of lamellae) can be observed surrounding rings constituted by flat-on crystals with low birefringence. The peculiar shape of lamellar edges has been associated to the intersection of the twisting lamellae and the spherulite surface [39].

In a previous work, FTIR microspectroscopic experiments were performed with a solution of P4HB crystallized spherulites which displayed a ringed texture in POM observations [19]. FTIR results showed a spherulitic sectorization when chemical images were obtained from integration of highly specific infrared peaks. Thus, only few bonds had a sufficiently different geometrical orientation to render a typical Maltese cross under polarizers. Chemical mapping was unable to show a ringed texture derived from a change of the orientation of selected chemical bonds along the spherulitic radius as could be expected for a twisted lamellar morphology. However, experimental limitations concerning a resolution limit that is very close to the interring spacing could not be discarded. Therefore, direct microscopy images obtained after selective removal of the amorphous regions were considered ideal to support the lamellar twisting in P4HB spherulites. Figure 5c reveals as the banded texture is defined after an appropriate exposure to enzymatic degradation media. Note that the bright field image showing the cropped out spherulites is fully consistent with the corresponding POM image (Figure 5d).

Controlling the exposure time and selecting the appropriate enzyme allows highlighting the spherulite morphology with high detail precision. Thus, SEM micrographs in Figure 6 shows the evolution of the initial sample, where bumps with diameters between 20-30 μm could be detected during exposure for 1, 2 and 3 days to the *Pseudomonas cepacia* enzymatic medium. The progressive erosion of the amorphous regions enables the

identification the banded structure, which began to be cropped after only 1 day (Figure 6b) and allows distinguishing the presence of edge lamellae at 2 days (Figure 6c). After that, images became unclear due to the presence of big crystals involving molecules produced during degradation (Figure 6d). Nevertheless, it is clear that erosion has clearly increased.

The sequence of degraded spherulites in the *Rhizopus oryzae* medium is shown in Figure 7. In this case, degradation advanced faster as it can be deduced by the comparison of images taken after 1 day (i.e., Figures 6b and 7a), when by-products of degradation caused less interferences in the visual aspect of the spherulites.

The performed assays indicated that the *Rhizopus oryzae* medium was the adequate one to visualize the spherulitic morphology and that after 3 days of exposure the crystalline texture of the spherulite was clearly delimitated. Figure 8a depicts a degraded spherulite where rings formed by cooperative C-shaped lamellar edges are highlighted. The magnification in Figure 8b enables the distinction of the main features of the two kinds of band: those mainly constituted by edge-on lamellae and those based of flat-on lamellae. Besides that, an abrupt lamellar twist seems to be produced, but similar effects have been reported for other systems indicating that lamellae curve smoothly despite the optical illusion [40].

CONCLUSIONS

Hydrolytic and enzymatic degradation of P4HB proceeds by following different mechanisms. Bulk degradation and a random chain scissions are characteristic of samples exposed to hydrolytic media, whereas surface erosion and depolymerization are characteristic of samples exposed to enzymatic media. Hydrolytic degradation rate can be controlled through the pH of the medium, being specifically enhanced in acidic media, and more significantly by increasing the temperature. Solubilization of degraded

fragments is significant in the enzymatic degradation due to its mechanism based on the successive removal of monomer units. Degradation processes affected predominantly to the amorphous regions, causing an increase on the degree of crystallinity as determined by DSC. Furthermore, the amorphous folds on the lamellar surface were more susceptible to degradation, leading to a slight change on the lamellar morphology. An increase on the lamellar width has been clearly inferred through DSC data by considering the increase on the melting temperature, and more directly by the analysis of SAXS correlation functions. Surface attack, high solubilization and high degradation rate (when appropriate enzymes with high activity are selected) are characteristics that enhance the interest towards the enzymatic process to crop out the morphologies of constitutive spherulites. In the present work, the enzymatic degradation has been successfully employed to show directly the structure of P4HB banded spherulites once the amorphous regions were selectively removed. SEM micrographs clearly pointed out an alternate disposition of edge-on and flat-of lamellae, and supported the theories based on a lamellar twisting.

Acknoledgements. The authors acknowledge support from MINECO and FEDER (RTI2018-101827-B-I00), and the Generalitat de Catalunya (2017SGR373). I.K. also acknowledges the financial support from B. Braun Surgical S.A. Diffraction experiments were performed at the NCD-SWEET beamlines at ALBA Synchrotron with the collaboration of ALBA staff.

REFERENCES

[1] D.P. Martin, S.F. Williams, Medical applications of poly-4-hydroxybutyrate: A strong flexible absorbable biomaterial, Biochem. Eng. J. 16 (2003) 97–105. https://doi.org/10.1016/S1369-703X(03)00040-8.

[2] S. Le Meur, M. Zinn, T. Egli, L. Thöny-Meyer, Q. Ren, Poly(4-hydroxybutyrate) (P4HB) production in recombinant Escherichia coli: P4HB synthesis is uncoupled with cell growth, Microb. Cell Fact. 12 (2013) 123. https://doi.org/10.1186/1475-2859-12-123.

[3] E.K. Odermatt, L. Funk, R. Bargon, D.P. Martin, S. Rizk, S.F. Williams, MonoMax suture: A new long-term absorbable monofilament suture made from poly-4-hydroxybutyrate, Int. J. Polym. Sci. 2012 (2012) 1–12. https://doi.org/10.1155/2012/216137.

[4] Tornier, announces Launch of BioFiber® Surgical Mesh for Tendon Repair at Arthroscopic Surgery Conference, Tornier Press Release. (2011). https://www.businesswire.com/news/home/20110414005940/en/Tornier-Announces-Launch-BioFiber®-Surgical-Mesh-Tendon.

[5] C.R. Deeken, B.D. Matthews, Characterization of the Mechanical Strength, Resorption Properties, and Histologic Characteristics of a Fully Absorbable Material (Poly-4-hydroxybutyrate-PHASIX Mesh) in a Porcine Model of Hernia Repair, ISRN Surg. 2013 (2013) 1–12. https://doi.org/10.1155/2013/238067.

[6] S.F. Williams, S. Rizk, D.P. Martin, Poly-4-hydroxybutyrate (P4HB): A new generation of resorbable medical devices for tissue repair and regeneration, Biomed. Eng. (NY). 58 (2013) 439–452. https://doi.org/10.1515/bmt-2013-0009.

[7] D.P. Martin, A. Badhwar, D. V. Shah, S. Rizk, S.N. Eldridge, D.H. Gagne, A. Ganatra, R.E. Darois, S.F. Williams, H.C. Tai, J.R. Scott, Characterization of poly-4-hydroxybutyrate mesh for hernia repair applications, J. Surg. Res. 184 (2013) 766–773. https://doi.org/10.1016/j.jss.2013.03.044.

[8] K. Mendelson, E. Aikawa, B.A. Mettler, V. Sales, D. Martin, J.E. Mayer, F.J. Schoen, Healing and remodeling of bioengineered pulmonary artery patches implanted in sheep, Cardiovasc. Pathol. 16 (2007) 277–282. https://doi.org/10.1016/j.carpath.2007.03.008.

[9] J. uwe Ackermann, S. Müller, A. Lösche, T. Bley, W. Babel, Methylobacterium rhodesianum cells tend to double the DNA content under growth limitations and accumulate PHB, J. Biotechnol. 39 (1995) 9–20. https://doi.org/10.1016/0168-1656(94)00138-3.

[10] L.F. Boesel, S. Le Meur, L. Thöny-Meyer, Q. Ren, The effect of molecular weight on the material properties of biosynthesized poly(4-hydroxybutyrate), Int. J. Biol. Macromol. 71 (2014) 124–130. https://doi.org/10.1016/j.ijbiomac.2014.04.015.

[11] D.H. Park, B.S. Kim, Production of poly(3-hydroxybutyrate) and poly(3-hydroxybutyrate-co-4-hydroxybutyrate) by Ralstonia eutropha from soybean oil, N. Biotechnol. 28 (2011) 719–724. https://doi.org/10.1016/j.nbt.2011.01.007.

[12] L. Zhang, Z.Y. Shi, Q. Wu, G.Q. Chen, Microbial production of 4-hydroxybutyrate, poly-4-hydroxybutyrate, and poly(3-hydroxybutyrate-co-4-hydroxybutyrate) by recombinant microorganisms, Appl. Microbiol. Biotechnol.

84 (2009) 909–916. https://doi.org/10.1007/s00253-009-2023-7.

[13] M. Martínez-Palau, L. Franco, X. Ramis, J. Puiggalí, Poly[(4-hydroxybutyric acid)-alt-(glycolic acid)]: Synthesis by thermal polycondensation of metal salts of 4-chlorobutyric acid carboxymethyl ester, Macromol. Chem. Phys. 207 (2006) 90–103. https://doi.org/10.1002/macp.200500260.

[14] F. Su, T. Iwata, K. Sudesh, Y. Doi, Electron and X-ray diffraction study on poly(4-hydroxybutyrate), Polymer (Guildf). 42 (2001) 8915–8918. https://doi.org/10.1016/S0032-3861(01)00412-8.

[15] F. Su, T. Iwata, F. Tanaka, Y. Doi, Crystal structure and enzymatic degradation of poly(4-hydroxybutyrate), Macromolecules. 36 (2003) 6401–6409. https://doi.org/10.1021/ma034546s.

[16] F. Tanaka, Y. Doi, T. Iwata, The deformation of the chain molecules and crystallites in poly([R]-3-hydroxybutyrate) and poly(4-hydroxybutyrate) under tensile stress, Polym. Degrad. Stab. 85 (2004) 893–901. https://doi.org/10.1016/j.polymdegradstab.2004.04.006.

[17] W.C. Hsieh, H. Mitomo, K.I. Kasuya, T. Komoto, Enzymatic degradation and aminolysis of microbial poly(3-hydroxybutyrate-co-4-hydroxybutyrate) single crystals, J. Polym. Environ. 14 (2006) 79–87. https://doi.org/10.1007/s10924-005-8710-2.

[18] I. Keridou, L.J. del Valle, L. Funk, P. Turon, I. Yousef, L. Franco, J. Puiggalí, Isothermal crystallization kinetics of poly(4-hydroxybutyrate) biopolymer,. Materials 12 (2019) 1–20. https://doi.org/10.3390/ma12152488.

[19] I. Keridou, L.J. Del Valle, L. Funk, P. Turon, L. Franco, J. Puiggalí, Non-isothermal crystallization kinetics of poly(4-hydroxybutyrate) biopolymer, Molecules. 24 (2019) 1–24. https://doi.org/10.3390/molecules24152840.

[20] P.J. Barham, A. Keller, E.L. Otun, P.A. Holmes, Crystallization and morphology of a bacterial thermoplastic: poly-3-hydroxybutyrate, J. Mater. Sci. 19 (1984) 2781–2794. https://doi.org/10.1007/BF01026954.

[21] T. Kyu, H.W. Chiu, A.J. Guenthner, Y. Okabe, H. Saito, T. Inoue, Rhythmic growth of target and spiral spherulites of crystalline polymer blends, Phys. Rev. Lett. 83 (1999) 2749–2752. https://doi.org/10.1103/PhysRevLett.83.2749.

[22] T. Teorell, E. Stenhagen, Universal buffer over the pH range 2.0 to 12.0., Biochem Z. (1938) 416–419.

[23] C.G. Vonk, G. Kortleve, X-ray small-angle scattering of bulk polyethylene, Kolloid Z Z Polym. 220 (1967) 19–24.

[24] C.G. Vonk, A general computer program for the processing of small-angle X-ray scattering data., J. Appl. Crystallogr. 8 (1975) 340–341.

[25] Z. Wang, G.C. Alfonso, Z. Hu, J. Zhang, T. He, Rhythmic growth-induced ring-banded spherulites with radial periodic variation of thicknesses grown from poly(ε-caprolactone) solution with constant concentration, Macromolecules. 41 (2008) 7584–7595. https://doi.org/10.1021/ma8005697.

[26] Y. Duan, Y. Jiang, S. Jiang, L. Li, S. Yan, Depletion-Induced Nonbirefringent Banding in Thin Isotactic Polystyrene Thin Films, Macromolecules. 37 (2004) 9283–9286.

[27] Y. Duan, Y. Zhang, S. Yan, J.M. Schultz, In situ AFM study of the growth of banded hedritic structures in thin films of isotactic polystyrene, Polymer (Guildf). 46 (2005) 9015–9021. https://doi.org/10.1016/j.polymer.2005.07.024.

[28] Y. Wang, C.M. Chan, L. Li, K.M. Ng, Concentric-ringed structures in polymer thin films, Langmuir. 22 (2006) 7384–7390. https://doi.org/10.1021/la060863r.

[29] B. Lotz, S.Z.D. Cheng, A critical assessment of unbalanced surface stresses as the mechanical origin of twisting and scrolling of polymer crystals, Polymer (Guildf). 46 (2005) 577–610. https://doi.org/10.1016/j.polymer.2004.07.042.

[30] I. Saracovan, J.K. Cox, J.F. Revol, R.S.J. Manley, G.R. Brown, Optically Active Polyethers. 3. on the Relationship between Main-Chain Chirality and the Lamellar Morphology of Solution-Grown Single Crystals, Macromolecules. 32 (1999) 717–725. https://doi.org/10.1021/ma971874h.

[31] B. Lotz, A. Thierry, Spherulite morphology of form III isotactic poly(1-butene), Macromolecules. 36 (2003) 286–290. https://doi.org/10.1021/ma021452u.

[32] H.D. Keith, F.J. Padden, Banding in polyethylene and other spherulites, Macromolecules. 29 (1996) 7776–7786. https://doi.org/10.1021/ma960634j.

[33] S. V. Meille, T. Konishi, P.H. Geil, Morphology of polypivalolactone: A polymer with a direction, Polymer (Guildf). 25 (1984) 773–777. https://doi.org/10.1016/0032-3861(84)90005-3.

[34] H.D. Keith, F.J. Padden, Twisting orientation and the role of transient states in polymer crystallization, Polymer (Guildf). 25 (1984) 28–42. https://doi.org/10.1016/0032-3861(84)90264-7.

[35] W. Cai, C.Y. Li, L. Li, B. Lotz, M. Keating, D. Marks, Submicrometer Scroll/Tubular Lamellar Crystals of Nylon 6,6, Adv. Mater. 16 (2004) 600–605. https://doi.org/10.1002/adma.200305634.

[36] B. Lotz, A. Thierry, S. Schneider, Molecular origin of the scroll-like morphology of lamellae in gamma PVF2 spherulites., Comptes Rendus Chim. 1 (1998) 609–614.

[37] D.C. Bassett, R.H. Olley, On the lamellar morphology of isotactic polypropylene spherulites, Polymer (Guildf). 25 (1984) 935–943. https://doi.org/10.1016/0032-3861(84)90076-4.

[38] S.S.N. Murthy, J. Sobhanadri, Study of some polyurethane elastomers using electrical methods, J. Appl. Polym. Sci. 54 (1994) 1499–1506. https://doi.org/10.1002/app.1994.070541014.

[39] J. Xu, H. Ye, S. Zhang, B. Guo, Organization of twisting lamellar crystals in birefringent banded polymer spherulites: A mini-review, Crystals. 7 (2017). https://doi.org/10.3390/cryst7080241.

[40] A. Lustiger, B. Lotz, T.S. Duff, The morphology of the spherulitic surface in polyethylene, J. Polym. Sci. Part B Polym. Phys. 27 (1989) 561–579. https://doi.org/10.1002/polb.1989.090270306.

Table 1. Melting peak temperatures and enthalpies of P4HB samples hydrolytically degraded at different pH values, temperatures and exposure times.

pH	*T* (ºC)	Time (days)	T_{m1}[a] (ºC)	T_{m2} (ºC)	ΔH_m[b] (J/g)
3	37	3	54.4	61.5	50.1
3	37	7	55.2	61.8	54.4
3	37	14	55.9	62.1	55.4
3	37	27	58.8	64.1	59.7
3	55	3	*47.7*	71.5	54.7
3	55	7	*47.8*	73.4	58.0
3	55	14	*50.1*	75.8	61.5
3	55	27	*50.7*	75.9	70.6
7	37	3	53.8	61.1	49.1
7	37	7	54.5	61.8	49.6
7	37	14	56.0	62.1	54.8
7	37	27	59.0	63.8	59.3
7	55	3	*47.9*	71.4	54.2
7	55	7	*47.9*	73.5	58.9
7	55	14	*49.2*	75.1	60.1
7	55	27	*51.4*	75.8	69.1
10	37	3	53.2	59.5	50.1
10	37	7	54.7	60.5	51.2
10	37	14	55.8	61.8	54.0
10	37	27	58.9	63.6	58.5
10	55	3	*47.9*	71.5	54.0
10	55	7	*48.0*	73.3	59.3
10	55	14	*48.7*	74.6	60.3
10	55	27	*53.5*	75.2	65.2

[a] Peaks of samples coming from 55 ºC are very broad and have small intensity. Probably correspond to highly defective crystals of distinct nature than those detected for samples exposed to 37 ºC. Peak temperatures are written in italics to point out this feature.
[b] Enthalpies corresponding to the main peak for degradations performed at 55 ºC and the global value for the shoulder and the main peak for degradations performed at 37 ºC.

Table 2. Melting peak temperatures and enthalpies of P4HB samples enzymatically degraded at a pH of 7.4, 37 ºC and different exposure times.

Enzyme	Time (days)	T_{m1}, T_{m2} (ºC)	ΔH_m[a] (J/g)
Pseudomonas cepacia	3	52.6, 61.7	54.7
Pseudomonas cepacia	7	52.7, 61.3	56.8
Pseudomonas cepacia	14	52.9, 61.5	56.9
Pseudomonas cepacia	21	53.4, 61.7	57.0
Rhizopus oryzae	3	53.6, 61.6	56.4
Rhizopus oryzae	7	53.5, 61.3	57.5
Rhizopus oryzae	14	54.3, 61.5	59.1
Rhizopus oryzae	21	54.2, 61.5	59.9

[a] Global enthalpy corresponding to the shoulder and the main peak.

Table 3. Lamellar morphological parameters of P4HB samples after being exposed to different degradation media.

Medium	pH	T (ºC)	Time (days)	L_γ (nm)	l_c (nm)	l_a (nm)	χ^{SAXS}
Original film	-	-	-	8.80	7.10	1.70	0.81
Hydrolytic	3	37	27	8.60	6.91	1.69	0.80
Hydrolytic	7	37	27	8.50	6.80	1.70	0.80
Hydrolytic	10	37	27	8.50	6.88	1.62	0.81
Hydrolytic	3	55	27	9.8	7.32	2.48	0.75
Hydrolytic	7	55	27	9.8	7.29	2.51	0.74
Hydrolytic	10	55	27	9.6	7.62	1.98	0.79
Pseudomonas cepacia	7.4	37	14	9.5	7.72	1.78	0.81
Pseudomonas cepacia	7.4	37	21	9.3	7.32	1.98	0.79
Rhizopus oryzae	7.4	37	14	9.6	7.25	2.35	0.76

FIGURE CAPTIONS

Figure 1. (a) Weight loss percentage versus exposure time to the hydrolytic degradation media at pH values of 3, 7 and 10 and temperatures at 37 ºC (dashed lines) and 55 ºC (solid lines). **(b)** M_n (o, □) and M_w (●, ■) molecular weights determined from GPC during degradation at the indicated pH values and temperatures. For the sake of completeness M_n values estimated from NMR spectra are also incorporated (◊) and specifically showed in the inset. **(c)** ^{1}H-NMR spectra of a P4HB melted film exposed to a pH 3 solution at 55 ºC for 27 days. Insets show the presence of terminal groups.

Figure 2. (a) SEM micrographs of P4HB films after being submitted to enzymatic degradation in a *Pseudomonas cepacia* (middle) and *Rhizopus oryzae* (right) media at 37 ºC for 21 days. A micrograph corresponding to a control (left) (degradation without enzyme in a pH 7.4 medium at 37 ºC) is also depicted for comparative purposes. **(b)** Weight loss percentage versus exposure time to enzymatic media containing lipases from *Pseudomonas cepacia* (0.1 mg/mL) and *Rhizopus oryzae* (0.072 mg/mL) at 37 ºC. **(c)** M_n (■) and M_w (☒) molecular weights determined from GPC during degradation at the indicated enzymatic media and temperature.

Figure 3. (a) DSC heating runs of P4HB hydrolytically degraded films after 3, 7, 14 and 27 days at 55 ºC and pH 10. Insets show the comparison between films degraded at 37 ºC and 55 ºC after 27 days of exposure at a pH 10 medium (left) and films degraded by exposure for 14 days to pH 3, pH 7 and pH10 media at 55 ºC (right). For the sake of comparison the DSC trace of the initial melt pressed sample is shown in the left inset. **(b)** DSC heating runs of P4HB enzymatically degraded films in a *Pseudomonas cepacia* medium after 21 days at 37 ºC. The inset shows, for the sake of completeness, the DSC

curves of samples exposed for 21 days to both enzymatic media and the comparison with the control.

Figure 4. SAXS correlation functions of P4HB films exposed for 27 days to aqueous medium of pH 3, pH 7 and pH 10 at 37 ºC **(a)** and 55 ºC **(b)**. Correlation function during enzymatic degradation exposed to two different lipases: *Pseudomonas cepacia* and *Rhizopus oryzae* **(c)** after 14 and 21 days. Insets show in all cases the corresponding 1D-SAXS profiles.

Figure 5. Optical micrographs showing P4HB thin films before **(a, b)** and after being exposed to a *Pseudomonas cepacia* (0.1 mg/mL) medium at 37 ºC **(c, d)** for 3 days. Images were taken without **(a, c)** and with polarizers **(b, d)** for the indicated days. Red and blue dashed ellipsoids point out spherulites before and after being exposed to the degradation medium.

Figure 6. SEM micrographs showing P4HB thin films before **(a)** and after being exposed to a *Pseudomonas cepacia* (1 mg/mL) medium at 37 ºC for 1 **(b)**, 2 **(c)** and 3 **(d)** days.

Figure 7. SEM micrographs showing P4HB thin films after being exposed to a *Rhizopus oryzae* (0.72 mg/mL) medium at 37 ºC for 1 **(a)**, 2 **(b)** and 3 days **(c)**.

Figure 8. SEM micrographs showing the details at different magnifications of a highlighted P4HB spherulite after exposure of a thin film to a *Pseudomonas cepacia* (1 mg/mL) medium for 3 days at 37 ºC.

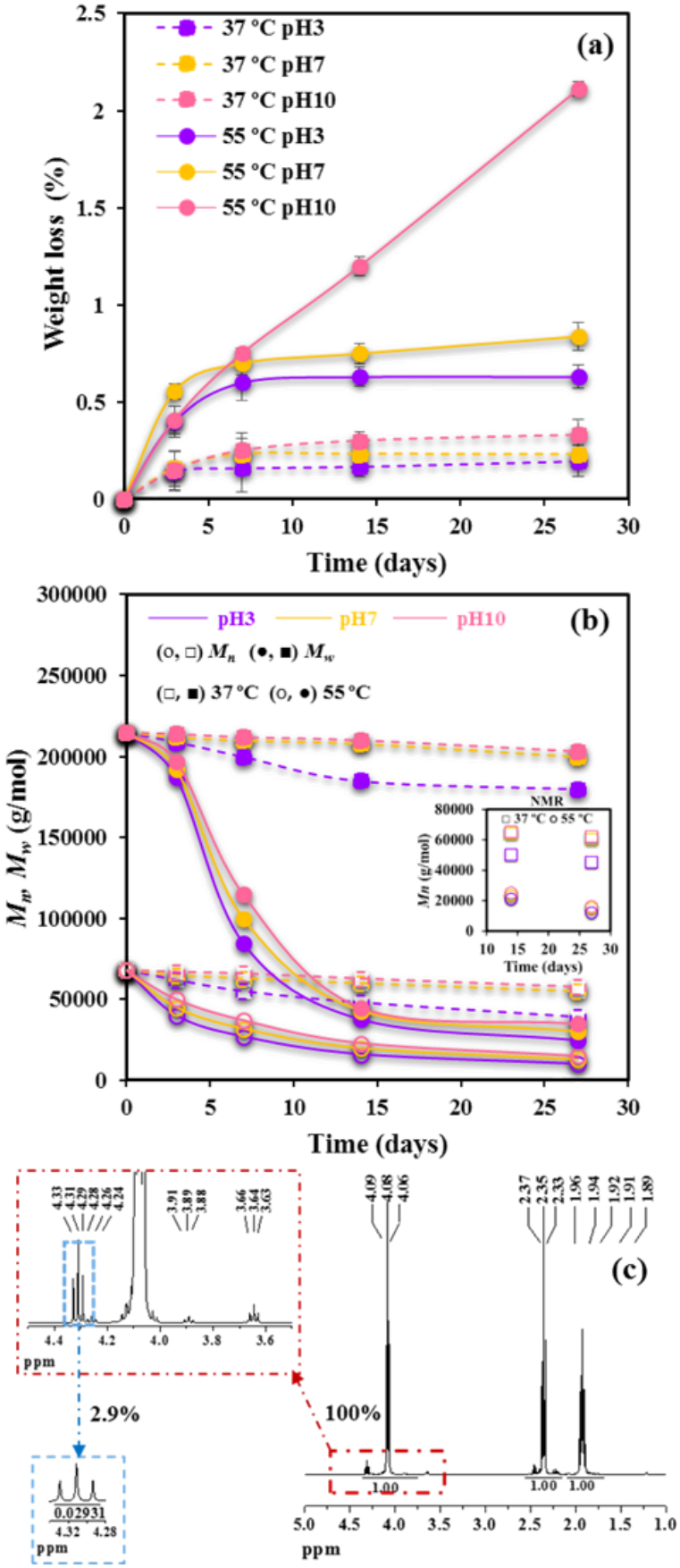

Figure 1

Keridou *et al.*

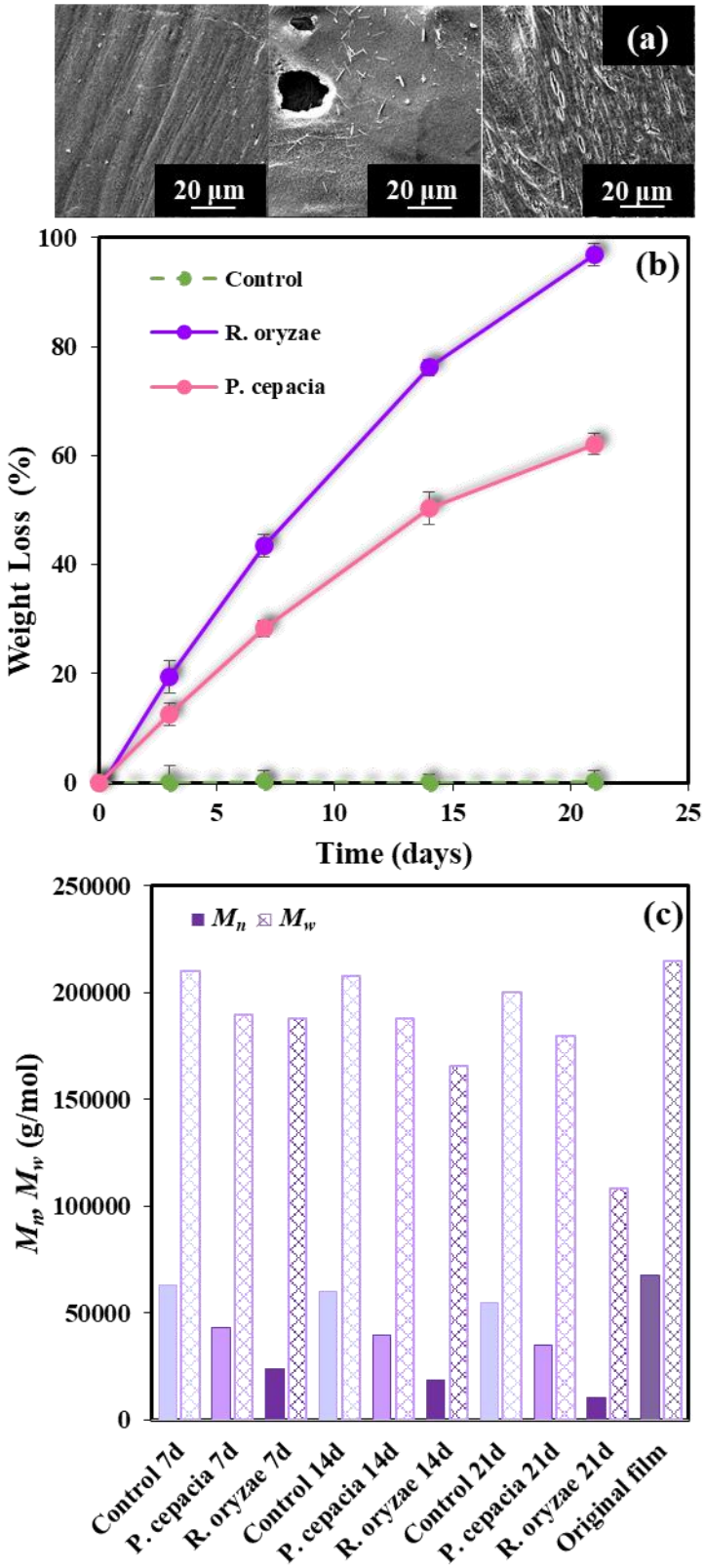

Figure 2

Keridou *et al.*

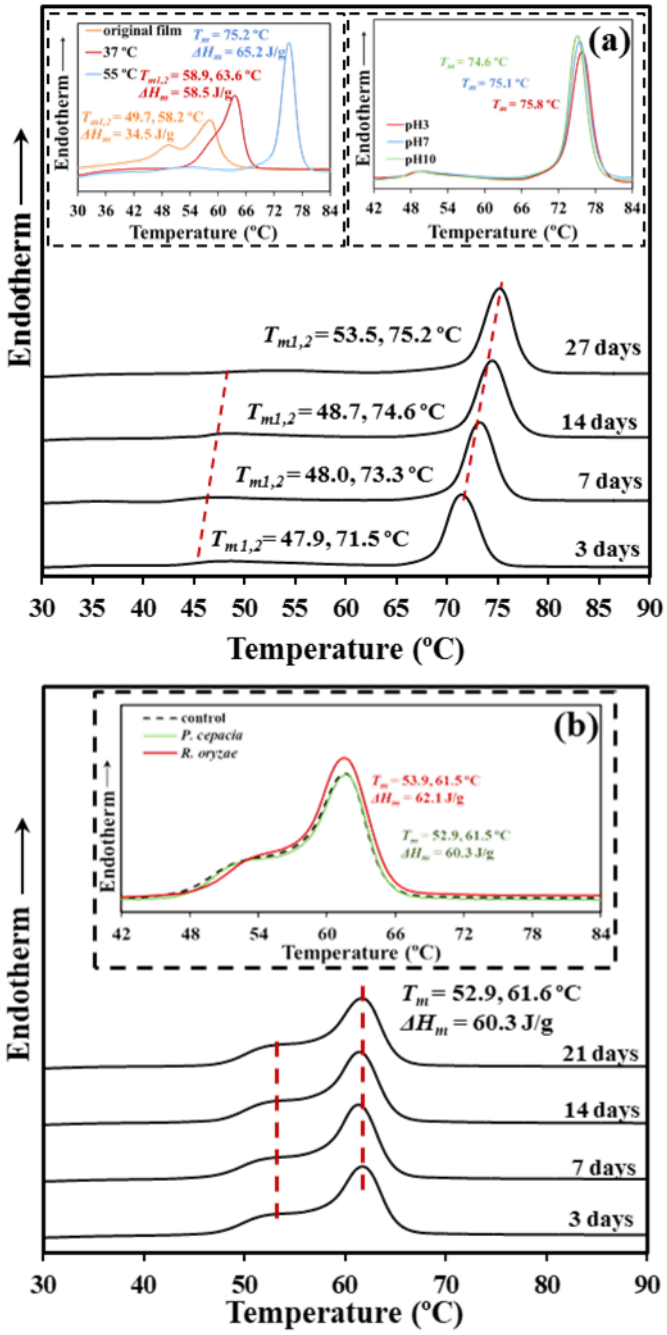

Figure 3

Keridou *et al.*

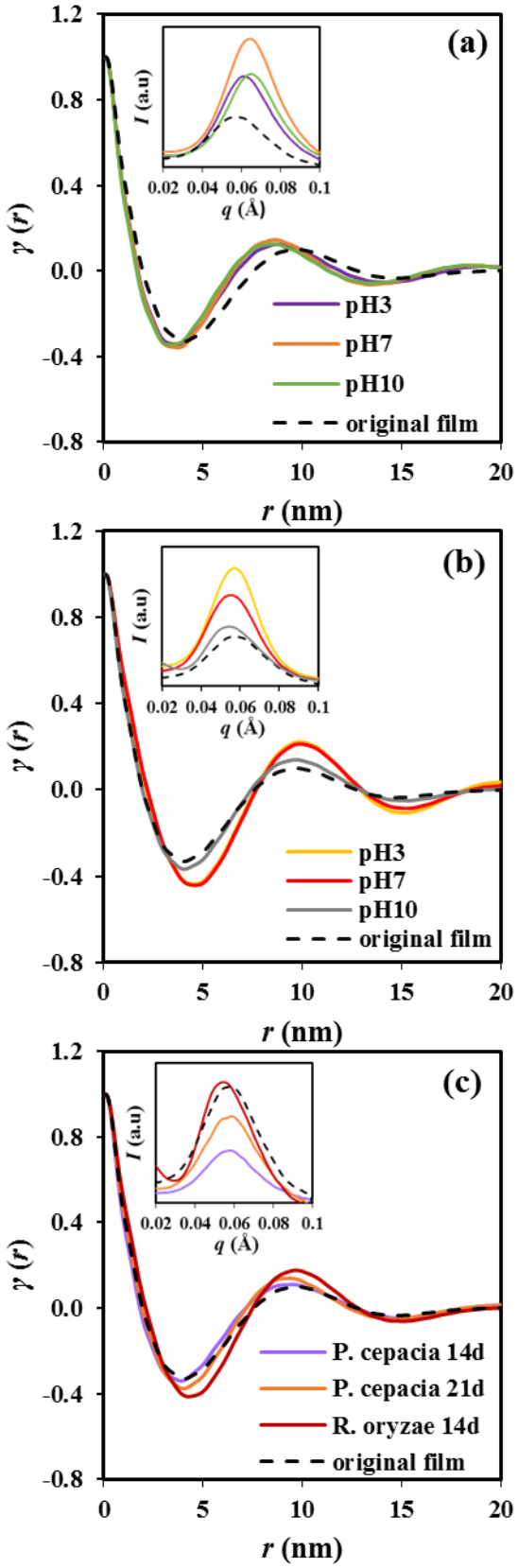

Figure 4

Keridou *et al.*

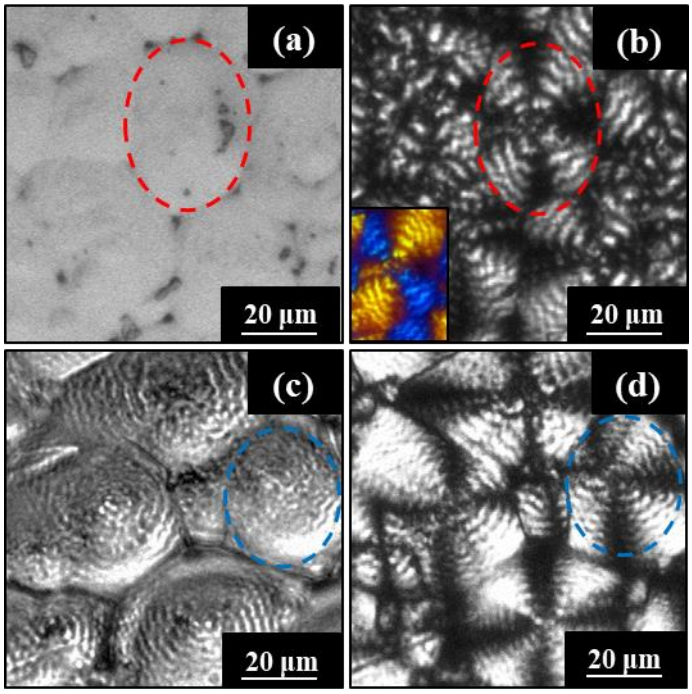

Figure 5

Keridou *et al.*

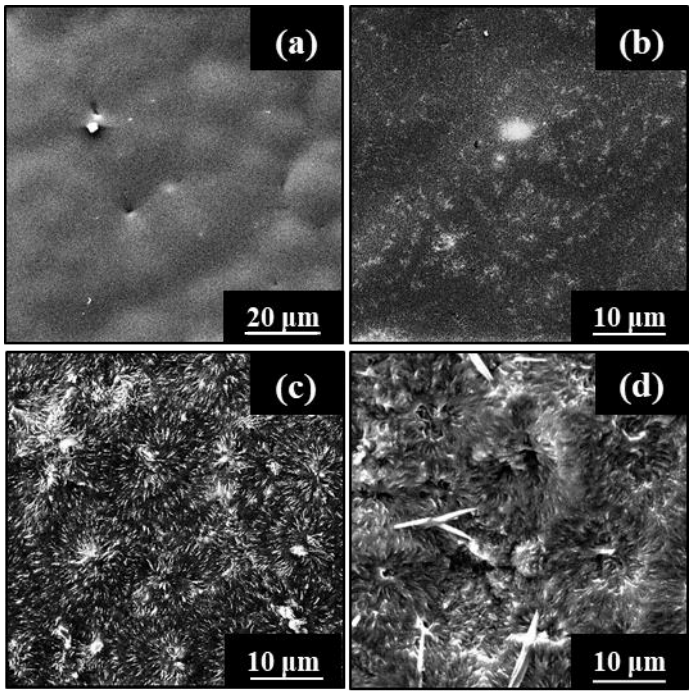

Figure 6

Keridou *et al*.

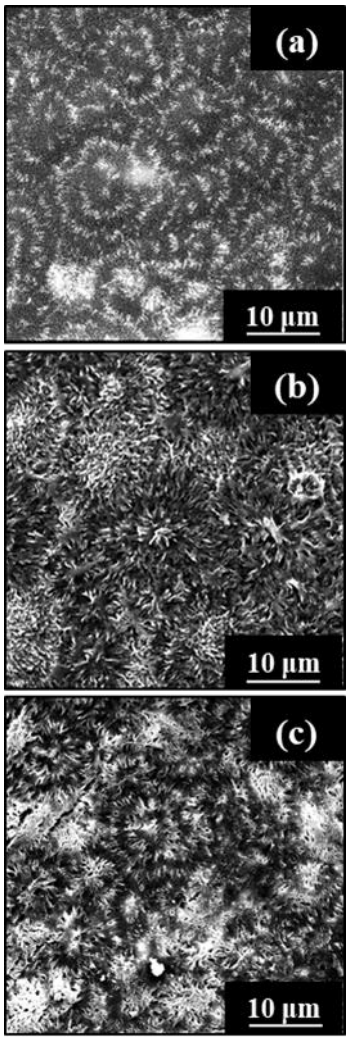

Figure 7

Keridou *et al*.

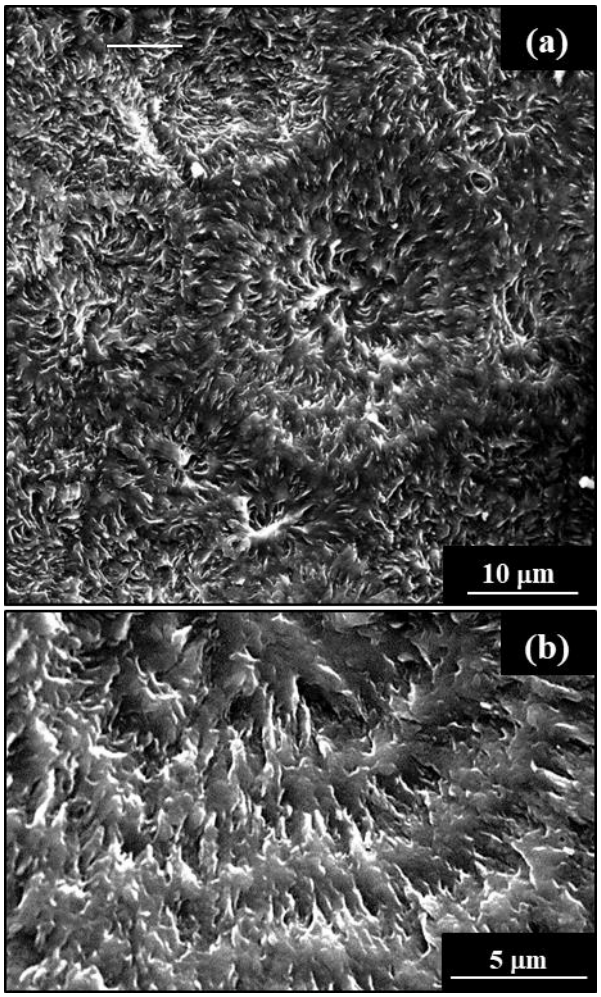

Figure 8

Keridou *et al*.